Erzgraber, H., Krauskopf, B., & Lenstra, D. (2006). Bifurcation analysis of a semiconductor laser with filtered optical feedback.

BIFURCATION ANALYSIS OF A SEMICONDUCTOR LASER WITH FILTERED OPTICAL FEEDBACK

HARTMUT ERZGRÄBER*, BERND KRAUSKOPF†, AND DAAN LENSTRA‡

Abstract. We study the dynamics and bifurcations of a semiconductor laser with delayed filtered feedback, where a part of the output of the laser re-enters after spectral filtering. This type of coherent optical feedback is more challenging than the case of conventional optical feedabck from a simple mirror, but it provides additional control over the output of the semiconductor laser by means of choosing the filter detuning and the filter width. This laser system can be modelled by a system of delay differential equations with a single fixed delay, which is due to the travel time of the light outside the laser.

In this paper we present a bifurcation analysis of the filtered feedback laser. We first consider the basic continuous wave states, known as the external filtered modes (EFMs), and determine their stability regions in the parameter plane of feedback strength versus feedback phase. The EFMs are born in saddle-node bifurcations and become unstable in Hopf bifurcations. We show that for small filter detuning there is a single region of stable EFMs, which splits up into two separate regions when the filter is detuned.

We then concentrate on the periodic orbits that emanate from Hopf bifurcations. Depending on the feedback strength and the feedback phase two types of oscillations can be found. First, there are undamped relaxation oscillations, which are typical for semiconductor laser systems. Secondly, there are oscillations with a period related to the delay time, which have the remarkable property that the laser frequency oscillates while the laser intensity is almost constant. These frequency oscillations are only possible due to the interaction of the laser with the filter. We determine the stability regions in the parameter plane of feedback strength versus feedback phase of the different types of oscillations. In particular, we find that stable frequency oscillations are dominant for nonzero values of the filter detuning.

Key words. Semiconductor laser, delayed feedback, optical filtering, delay differential equation, bifurcation analysis

AMS subject classifications. 15A15, 15A09, 15A23

1. Introduction.

Semiconductor lasers are very efficient sources of coherent light that are used in countless technical applications — most notably in optical data storage and optical communications systems. A single-mode semiconductor laser on its own is mathematically a damped nonlinear oscillator. An important source of nonlinearity is a strong coupling between the light intensity and the output frequency. Furthermore, due to the high efficiency of the semiconductor material, the reflectivity of the mirrors of semiconductor lasers is very low (only about 30 %). Therefore, this type of laser is very susceptible to external influences: external light can enter easily and disturb the delicate balance inside the laser; see, for example, [19, 21] as an entry point to the extensive literature on semicondutor laser dynamics.

From a dynamical systems point of view, semiconductor laser systems are very attractive because they show an intriguing variety of complicated dynamics. Furthermore, it is known that their description, by relatively simple mathematical models, is

*Afdeling Natuurkunde en Sterrenkunde, Vrije Universiteit Amsterdam, De Boelelaan 1081, 1081 HV Amsterdam, The Netherlands (h.erzgraber@few.vu.nl).

†Department of Engineering Mathematics, University of Bristol, Bristol BS8 1TR, UK (b.krauskopf@bristol.ac.uk). The work of this authors was supported by an Engineering and Physical Sciences Research Council (EPSRC) Advanced Research Fellowship grant.

‡Afdeling Natuurkunde en Sterrenkunde, Vrije Universiteit Amsterdam, De Boelelaan 1081, 1081 HV Amsterdam, The Netherlands, and Research Institute COBRA, Technical University Eindhoven, The Netherlands (lenstra@nat.vu.nl).

in very good agreement with experimental measurements [32].

In applications it is impossible to completely isolate a laser from external light. Therefore, one has to find ways to minimize or control the effects of external optical perturbations. Furthermore, one often wants to control the output characteristics of the laser, for example, to ensure constant intensity output at a desired frequency. On the other hand, there is the possibility to make use of chaotic dynamics of SLs, for example, as a chaotic carrier wave for secure communication or to produce highly efficient incoherent light sources.

Different schemes have been proposed for controlling the dynamics of semiconductor lasers, including optical injection of light from a second laser [32], and different types of optical feedback [19]. The simplest optical feedback scheme is conventional optical feedback (COF), where the laser receives feedback from a normal mirror. However, other types of feedback are also possible, including optical feedback from two different mirrors [28], incoherent feedback [7], phase-conjugate feedback (PCF) [1, 10], and optoelectronic feedback [25].

In this paper we consider a semiconductor laser subject to filtered optical feedback (FOF) where the reflected light is spectrally filtered before it re-enters the laser. This coherent optical feedback system, which is known as the FOF laser, has recently been the subject of a number of experimental and theoretical studies. As in any optical feedback system, important parameters are the delay time and the feedback rate. Moreover, for coherent feedback, there is also a feedback phase that controls the phase of the incident light. The interest in the FOF laser is due to the fact that filtering of the reflected light allows additional control over the behavior of the laser by means of choosing the filter detuning (the difference between the central filter frequency and the free-running laser frequency) and the filter width.

A particular motivation for the bifurcation analysis performed here was the discovery by *Fischer et. al.* [9] of a new type of oscillations. These, the so-called frequency oscillations (FOs), which are characterized by oscillations of the optical frequency of the laser while its intensity remains practically constant. Mathematically this means that the dynamics of the laser takes place in a very small neighborhood of a cylinder in phase space. The existence of FOs is remarkable for several reasons. First, pure FOs are 'unusual' for semiconductor lasers due to the strong amplitude-phase coupling in these lasers. Second, the period of the FOs is on the order of the delay time of the FOF system, while one would normally expect the undamping of the characteristic relaxation oscillations (ROs) to be the first instability to be encountered in semiconductor lasers. Note that ROs are a well-known feature of laser dynamics. Specifically, they are a periodic exchange of energy between the optical field (the number of photons) and the population inversion (the number of electron-hole pairs) of the laser. They have a characteristic frequency that depends on the laser and its operating conditions and is in the order of GHz [33].

We present here a detailed bifurcation study, where we identify the stability regions of the basic solutions of the FOF laser, the external filtered modes or EFMs, and of the different types of bifurcating oscillations, ROs and FOs. We present this information in the plane of feedback strength versus feedback phase, for different values of the filter detuning. This amounts to a study of a physically relevant part of a three-dimensional parameter space.

Laser systems involving optical feedback, such as the FOF laser considered here, are quite challenging to analyse because they need to be modelled by delay differential equations (DDEs), which feature an infinite-dimensional phase space. In this

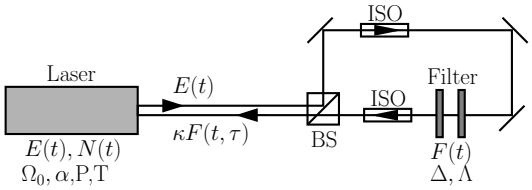

FIG. 2.1. *FOF laser set-up with a Fabry-Pérot filter in a loop with optical isolators (ISO).*

work we use numerical continuation software for DDEs, namely the packages DDE-BIFTOOL [4] and PDDE-CONT [30], to find and follow EFMs and periodic orbits (corresponding to FOs and ROs) and to determine their stability and bifurcations.

We finish this introduction with a brief review of other work on the FOF laser. Experimental studies in comparison with results from numerical integration of the governing rate equations can be found in [8, 34, 35]. As was mentioned, FOs were first found in an experiment reported in [9]. An initial investigation of their stability in comparison with experimental data can be found in [6]. An analytical treatment of the EFMs is presented in [12]. The connection between FOF and optical injection is the subject of [5, 17], while [18] considers different limits of the FOF laser equations. A reduced model for weak FOF is derived, analysed and compared with the full model in [27]. All of these papers consider the case of a filter with a single maximum in its reflectivity (as a function of the frequency). A filter with a minimum at its center frequency is the subject of [31], where continuous wave solutions and bifurcating periodic orbits are determined in a rate equation model.

This paper is organized as follows. In Section 2 we present details of the FOF laser and, in particular, the governing DDE model. Section 3 presents the stability regions of the EFMs, which includes a detailed analysis of how the stability region splits into two parts when the filter is detuned. In Section 4 we characterize ROs and FOs and determine their stability regions in the plane of feedback strength versus feedback for different values of the detuning. Finally, we summarize and point to future work in Section 6.

2. The FOF laser system. There are a number of ways to set up a frequency selective element in optics [16], including Michealson Interferometers, optical gratings, or Fabry-Pérot cavities. Figure 2.1 shows a looped set-up that has been used in experiments [8]. A fraction of the laser's emission travels through a Fabry-Pérot filter before the light is fed back into the laser. Optical isolators ensure that there are no unwanted reflections.

The FOF laser can be modelled by rate equations for the complex optical field E of the laser, the (real) population inversion N of the laser, and the complex optical field F of the filter. In dimensionless form these equations can be written as

$$\frac{dE}{dt} = (1 + i\alpha)N(t)E(t) + \kappa F(t,\tau)\,, \tag{2.1}$$

$$T\frac{dN}{dt} = P - N(t) - (1 + 2N(t))|E(t)|^2\,, \tag{2.2}$$

$$\frac{dF}{dt} = \Lambda E(t-\tau)e^{-iC_p} + (i\Delta - \Lambda)F(t)\,. \tag{2.3}$$

Here the material properties of the laser are given by the linewidth enhancement factor α and the electron life-time T, while P is the pump rate.

The laser is coupled to the filter in Eq. (2.1) via the coupling term $\kappa F(t,\tau)$, where κ is the feedback rate and τ is the delay time that arises from the finite propagation time of the light in the external feedback loop. Equation (2.3) for the complex envelope F of the filter field is derived by assuming a single Lorentzian approximation for the Fabry-Pérot filter; see, for example, [11, 26] for details. The feedback phase C_p in Eq. (2.3) measures the exact phase relationship between the laser and the filter fields, whereas Δ is the detuning between the filter center frequency Ω_F and the solitary frequency Ω_0 of the laser, that is,

$$C_p = \Omega_0 \tau\,, \quad \Delta = \Omega_F - \Omega_0\,. \tag{2.4}$$

Finally, the parameter Λ is the filter width (half-width at half-maximum).

Throughout this paper, we fix some of the parameters at the physically realistic values $\alpha = 5.0$, $T = 100$, $P = 3.5$, $\tau = 500$ and $\Lambda = 0.007$. The parameters κ and C_p are our main bifurcation parameters, that is, we consider the bifurcation diagram in the (κ, C_p)-plane. Furthermore, we study how the bifurcation diagram changes with the filter detuning Δ.

Mathematically, Eqs. (2.1)–(2.3) are a system of DDEs with a single fixed delay τ. As such, they have as phase-space the infinite-dimensional space of continuous functions over the delay interval $[-\tau, 0]$ with values in (five-dimensional) (E, N, F)-space. This infinite-dimensionality of the system makes its analysis quite challenging. Nevertheless, stability and bifurcation theory for DDEs with fixed delays is well developed [2, 15]. Furthermore, numerical bifurcation tools are now becoming available that allow one to find and follow equilibria and periodic solutions and some of their bifurcations; see the review [19].

As is common for optical feedback systems (with the exception of phase conjugation) [23], Eqs. (2.1)–(2.3) have an S^1-symmetry, given by any rotation of both E and F:

$$(E, F, N) \to (Ee^{ib}, Fe^{ib}, N)\,. \tag{2.5}$$

In other words, solutions are not isolated, which must be taken into account in the numerical continuation; see [14, 19]. Furthermore, there is the trivial 2π-translational symmetry

$$(E, F, N, C_p) \to (E, F, N, C_p + 2\pi)\,, \tag{2.6}$$

in the feedback phase C_p. We already remark that it is convenient to represent bifurcation diagrams on the covering space $\mathbb{R}$ of C_p, that is, over several 2π-intervals.

3. External filtered modes. The external filtered modes are the basic solutions of Eqs. (2.1)–(2.3) that correspond to a constant-intensity output of the laser. They are conceptially the same as the external cavity modes of the COF laser [11, 29]. Mathematically, the EFMs are group orbits of the S^1-symmetry (2.5 of the form

$$(E(t),\, N(t),\, F(t)) = (E_s e^{i\omega_s t},\, N_s,\, F_s e^{i\omega_s t + i\phi})\,. \tag{3.1}$$

Here ω_s is a fixed frequency, $E_s \geq 0$ and $F_s \geq 0$ are fixed (real) values of the field amplitude of the laser field and the filtered field, N_s is a fixed level of inversion, and ϕ is a fixed phase shift between the laser field and the filtered field. In other words, the system outputs light with frequency ω_s and constant intensity $I_s = E_s^2$.

An analytical study of the EFMs and their dependence on the filter detuning Δ and filter width Λ has been performed in [11]. Depending on the values of these

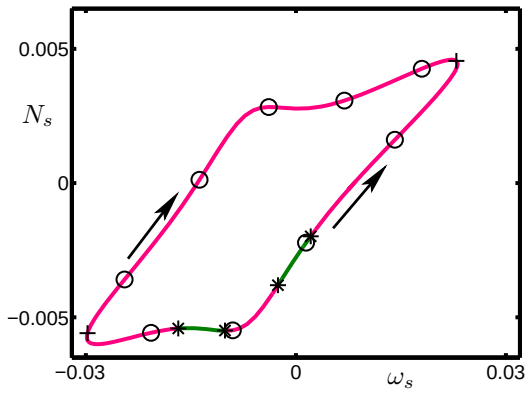

FIG. 3.1. *EFM-component in the (ω_s, N_s)-projection for a small negative detuning of $\Delta = -0.007$. Individual EFMs for $C_p = \pi$ are plotted as circles ($\circ$). The EFMs trace out the underlying curve or EFM-component as C_p is decreased, as is indicated by the arrows; see also the accompanying animation* `ekl_a1.gif`. *Stable parts of the EFM-component are plotted green and unstable parts red. EFMs are born and destroyed in saddle-node bifurcations ($+$); Hopf bifurcations ($*$) bound the stable parts.*

parameters the ECMs lie on one or two closed curves in the (ω_s, N_s)-projection, which are known as EFM-components. The number of EFM-components can be derived from a fourth-degree polynomial. We remark that stability properties of EFMs were not considered in [11].

In this paper we perform a bifurcation analysis of EFMs, determine how their stability depends on parameters, find stability boundaries, in particular, Hopf bifurcations, and study the stability of bifurcating periodic orbits. To this end, we use numerical continuation, namely the software package DDE-BIFTOOL [4], to analyse the full DDE (2.1)–(2.3). Some stability curves of peridic orbits are computed with the package PDDE-CONT [30].

Figure 3.1 shows EFMs on a single EFM-component in the (ω_s, N_s)-projection (for $C_p = \pi$). This projection is popular in the laser physics literature, even though neither ω_s nor N_s are parameters of the system. As C_p is decreased, the EFMs trace out the closed curve — the EFM-component — as is indicated by the arrows. The EFM-component has a 'bulge' around the center frequency of the filter, which is detuned slightly, in negative the negative direction with respect to the solitary laser frequency. EFMs are born in pairs in saddle-node ($+$) bifurcations in the low-inversion region, move along the EFM-component and then disappear in a second saddle-node in the high-inversion region. When C_p is decreased by 2π, each EFM has moved to the position of its right neighbor and the initial picture is recovered; see also the accompanying animation `ekl_a1.gif`.

Figure 3.1 also contains the stability information of the EFMs, namely they are stable along the green parts and unstable along the red parts of the EFM-component. The stability regions are bounded by Hopf bifurcations ($*$), which may lead either to stable relaxation oscillations or frequency oscillations as will be discussed in Section 4. Note that there are additional Hopf bifurcations of already unstable EFMs, which we did not plot in order to to keep the figure simple. Figure 3.1 already indicates that there are values of C_p for which more than one EFM is stable.

To bring out this point better, Fig. 3.2 shows the EFMs in the (κ, N_s)-projection

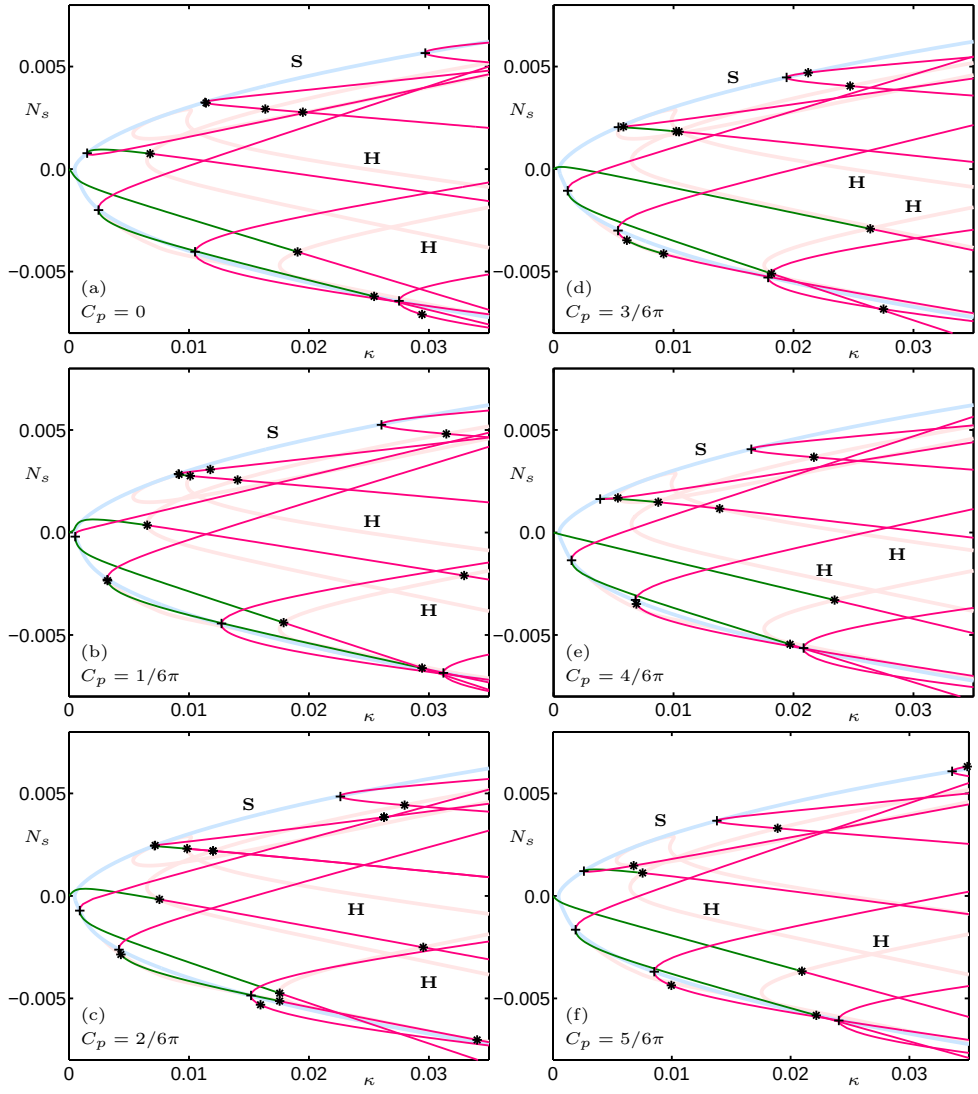

FIG. 3.2. *The EFMs in the (κ, N_s)-projection for six different values of C_p as indicated in the panels, and for a small negative detuning of $\Delta = -0.007$; same conventions for stability and bifurcations as in Fig. 3.1. In addition, lines of saddle-node bifurcations (light blue) and Hopf bifurcations (light red) are plotted. As C_p is changed each bifurcation follows its respective curve; see also the accompanying animation* `ekl_a2.gif`.

for six different values of the feedback phase C_p. In other words, we now plot actual branches of EFMs as a function of the parameter κ. For small feedback rates, close to zero, only one EFM exists, which is actually (the continuation of) the stable solitary laser mode. As κ is increased, new EFMs are born in pairs in saddle-node bifurcations. One of these EFMs may be stable (green parts of the curve). As the feedback rate κ is increased further, stable EFMs destabilize in Hopf bifurcations. The different panels of Figure 3.2 show the EFM structure for six different values of C_p over one cycle of 2π. As a function of C_p the branches of EFMs move until the same situation

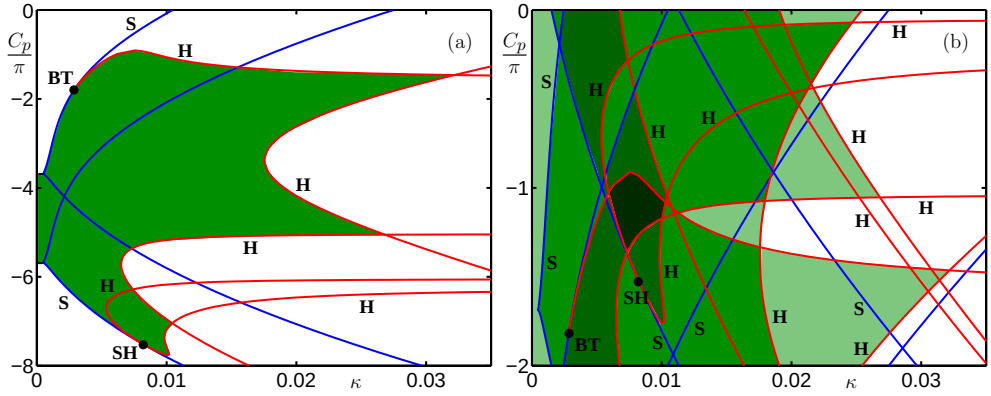

FIG. 3.3. *Two-parameter bifurcation diagram in the (κ, C_p)-plane for a small nonzero detuning of $\Delta = -0.007$. Saddle-node bidurcation curves (S) are blue, Hopf bifurcation curves (H) are red, and regions of stable EFMs are green. Codimension-two Bogdanov-Takens (BT) and saddle-node Hopf points (SH) are indicated by dots. Panel (a) shows the bifurcation diagram in the covering space (over several 2π intervals of C_p), while panel (b) shows it on a fundamental 2π-interval of C_p. Different shades of green indicated regions of different numbers of simultaneously stable EFMs.*

is regained after C_p has been changed over 2π. During this cyclic process, the saddle-node bifurcations trace out the light blue curve and the Hopf bifurcations the light red curves, respectively; see also the accompanying animation `ekl_a2.gif`. Note that tracing out all EFMs branches over an interval of 2π in C_p is equivalent to tracing out a single EFM branch over several intervals of 2π in the covering space.

3.1. Stability regions of the external filtered modes. The stability information of EFMs for $\Delta = -0.007$ is presented in Figure 3.3 as a two-parameter bifurcation diagram in the (κ, C_p)-plane. In panel (a) the bifurcation diagram is shown in the covering space of C_p over several cycles of 2π. The green stability region of EFMs is bounded by saddle-node bifurcations (blue curves) and by Hopf bifurcations (red curves). At codimension-two Bogdanov-Takens (BT) and saddle-node (SH) Hopf bifurcation points the nature of the stability boundary changes from saddle-node to Hopf bifurcation. At the Bogdanov-Takens point the Hopf curve ends and the frequency of the associated periodic orbit goes to zero. On the other hand, at the saddle-node Hopf point the saddle-node and Hopf curves are tangent and change from supercritical to subcritical; the frequency of the accociated periodic orbits is finite. We refer to [13, 24] for background reading on bifurcation theory. The stability boundary is formed to the right by a total of four different Hopf bifurcation curves, which intersect at double-Hopf bifurcation points.

The bifurcation diagram shown in Figure 3.3(a) is only one of infinitely many copies under the 2π translation symmetry of C_p. To reveal the considerable degree of multistability of EFMs that was already apparent from Fig. 3.2, we show in Figure 3.3(b) the stability regions of all EFMs over a fundamental 2π-interval of C_p. (Note that the top and bottom of panel (b) can be glued together to obtain a bifurcation diagram on the half-cylinder $S^1 \times \mathbb{R}^+$.) While panel (b) clearly shows the multistability of the system; a representation of the bifurcation diagram in the covering space as in panel (a) is more convenient for distinguishing bifurcation curves that make up the stability boundary.

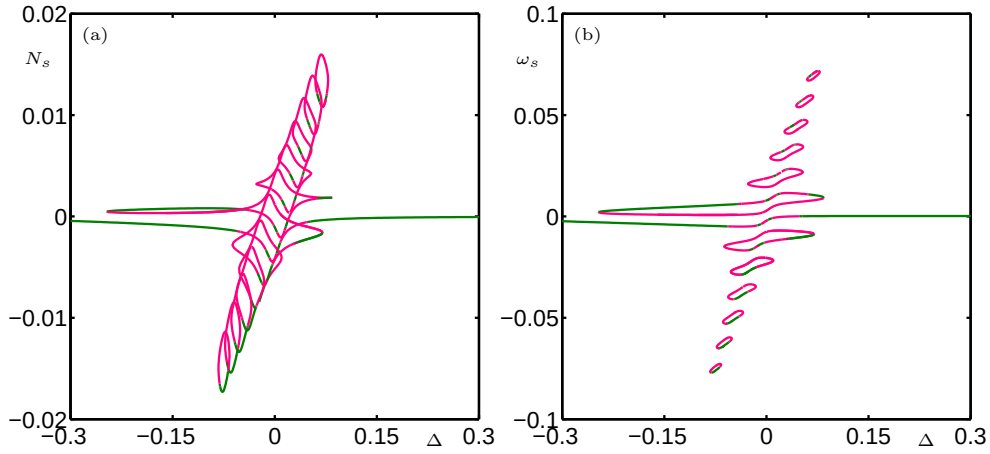

FIG. 3.4. *One-parameter bifurcation diagrams showing branches of EFMs as a function of* Δ *for fixed* $\kappa = 0.02$*. Panel (a) shows the* N_s*-values and panel (b) the* ω_s*-values of the EFMs; stable parts are green and unstable parts are red.*

3.2. Dependence of EFM stability on the detuning. We now consider what effect the influence of the detuning Δ has on the stability of the EFMs. We start with the one-parameter bifurcation diagram in Fig 3.4, where the N_s- and ω_s-values of the EFMs are shown as a function of Δ for fixed $\kappa = 0.02$. The EFM originating from the solitary laser solution exists for all values of Δ and forms a single branch. For large positive and negative detunings (when there is effectively no feedback any more) it apprwoaches $N_s = 0$ and $\omega_s = 0$, respectively. Around zero Δ additional EFMs exist on isolas (closed curves) that are bounded by saddle-node bifurcations. For each fixed Δ there are finitely many EFMs that lie either on a single EFM component (as in Fig 3.1) on on two separate EFM-components; compare [11].

We now discuss global aspects that a change of the detuning Δ has on stability of EFM stability regions. Representative bifurcation diagrams in the (κ, C_p) are shown in Figs. 3.5 and 3.6; see also the accompanying animation `ekl_a3.gif`. Specific details of transitions through codimension-three points are discussed in Sec 3.3.

Figure 3.5 shows bifurcation diagram in the (κ, C_p)-plane for eight different values of positive detuning from $\Delta = 0$ to $\Delta = 0.0735$. In the individual panels only those Hopf bifurcation curves are shown that form part of the EFM stability boundary and those that become relevant as the detuning changes. For $\Delta = 0$ in panel (a) the EFM stability region is almost symmetric, which indicates only a weak influence (on the EFM structure) of the phase-amplitude coupling expressed by the parameter α. Note that the boundary changes from a saddle-node bifurcation curve to a Hopf bifurcation curve at two saddle-node Hopf points. With increasing Δ the overall shape of the stability region changes and becomes less symmetrical. Already for $\Delta = 0.007$ in panel (b) the Hopf curve forming the lower boudary of the EFM stability region ends in a Bogdanov-Takens point, as was discussed above. The nature of this change from a saddle-node Hopf to a Bogdanov-Takens point is discussed in more detail in Sec 3.3.

Increasing Δ, the stability region deforms further until, at $\Delta \approx 0.014$, it splits into two parts; see Fig. 3.5(d). This transition is due to a transition through a codimension-three degenerate saddle-node Hopf bifurcation, as is discussed in more

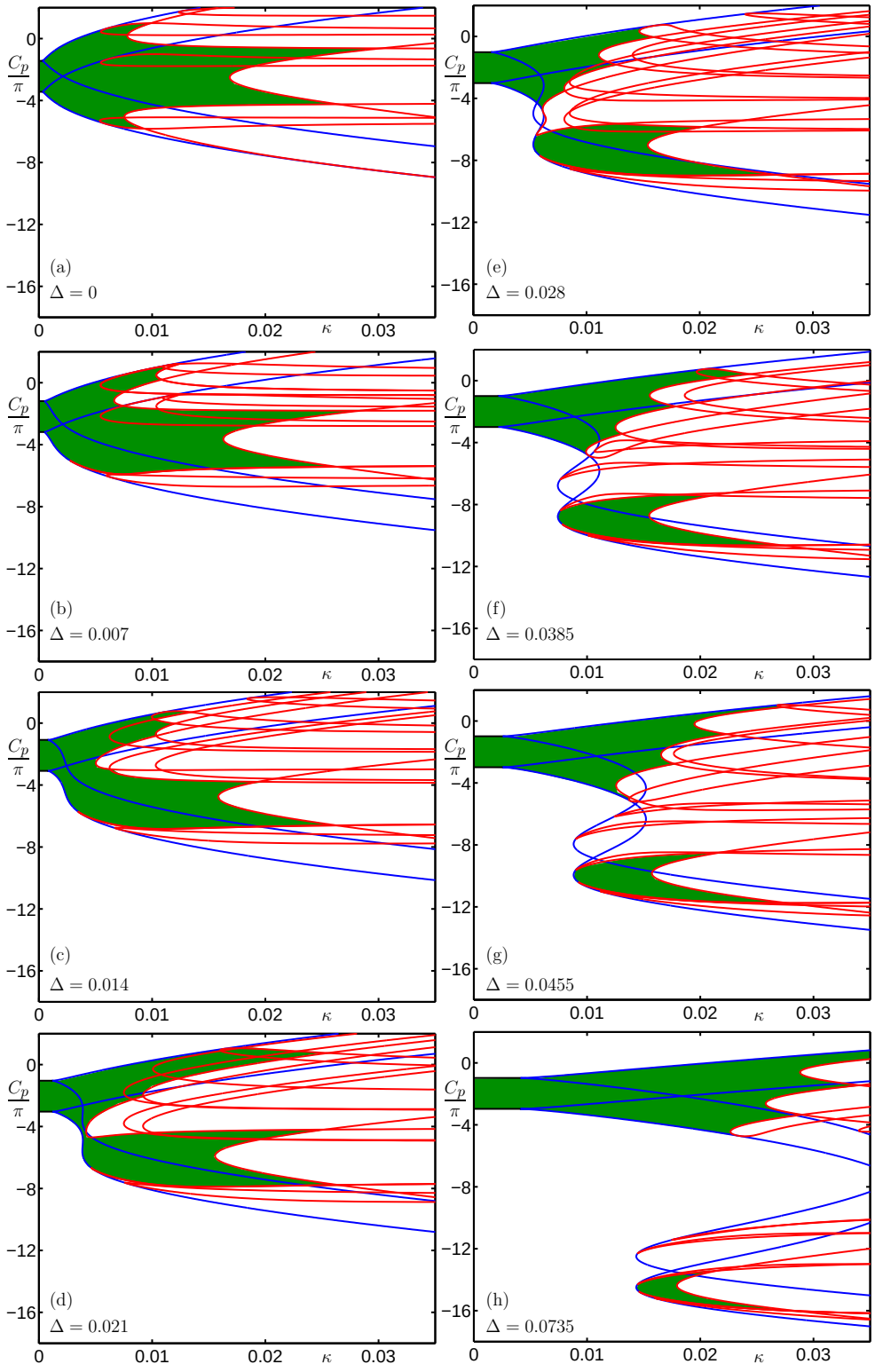

FIG. 3.5. *Two-parameter bifurcation diagram in the (κ, C_p)-plane for increasing detuning Δ as inducated in the panels; see also the accompanying animation* `ekl_a3.gif`. *Curves and regions are colored as in Fig. 3.3.*

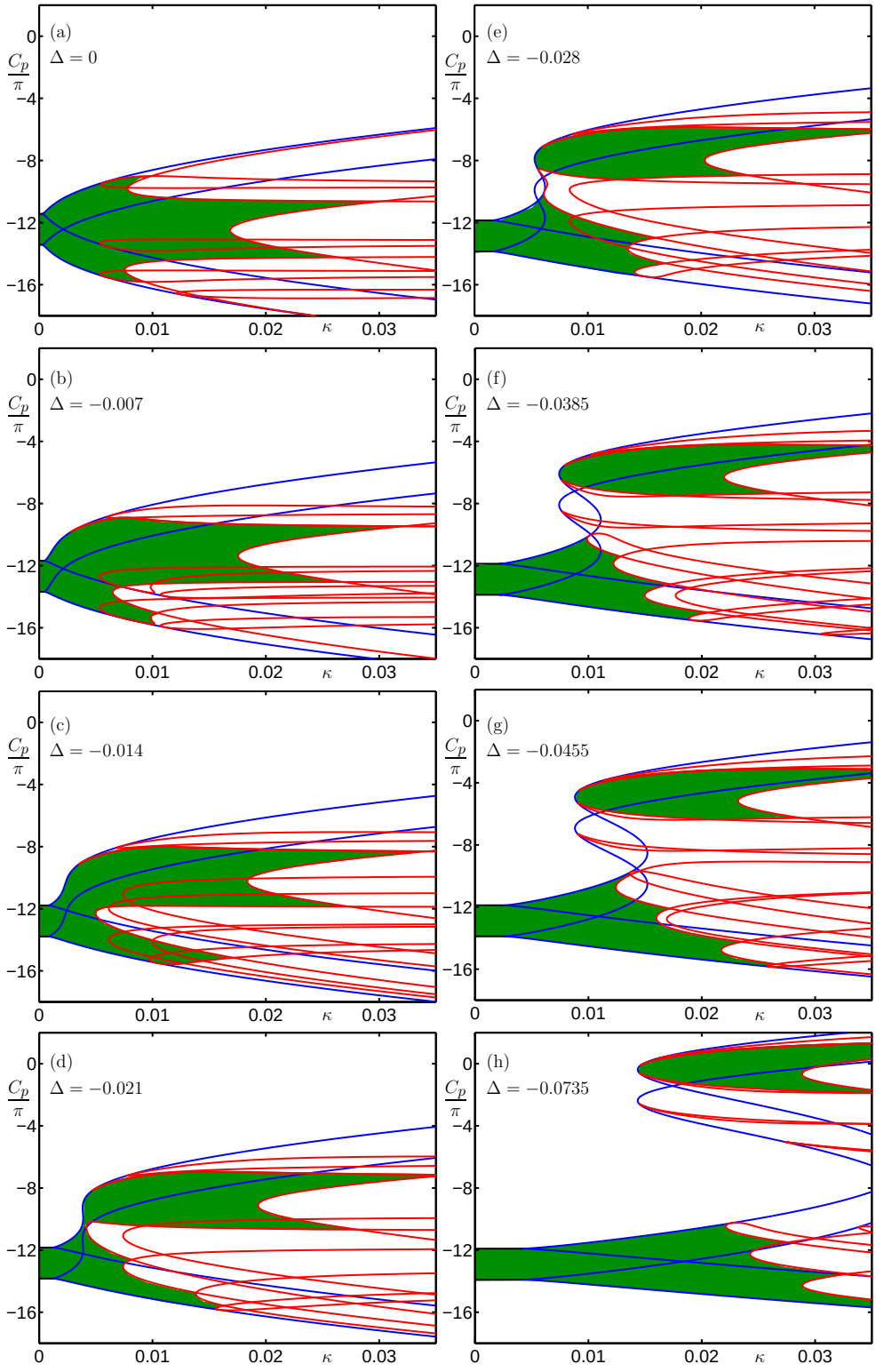

FIG. 3.6. *Two-parameter bifurcation diagram in the (κ, C_p)-plane for decreasing detuning Δ as indicated in the panels; see also the accompanying animation* `ekl_a3.gif`. *Curves and regions are colored as in Fig. 3.3.*

detail in Sec 3.3. For even higher values of Δ the EFM stability region consists of two parts; see panels (e)–(h). It is known that there is a boundary curve in the (Λ, Δ)-plane inside of which one finds two distinct EFM-components. Furthermore, this curve scales linearly with the feedback rate κ [11]. The two separate EFM stability regions have different physical meanings, one corresponds to operation of the laser around its solitary frequency and the other to operation around the filter frequency. Note that, irrespective of their stability, EFMs exist in the whole area bounded by the saddle-node curves.

However, for small κ stable EFMs are only possible around the solitary laser frequency (around $C_p = -2\pi$ in panels (e)–(h)). For higher values of κ also EFMs around the center frequency of the filter may also be stable. These form an 'island' of stable EFMs. Further increasing Δ separates the two stability regions. Specifically, the island of EFMs located around the center frequency of the filter moves down in the (κ, C_p)-plane and simultaneously becomes smaller in size; see panels (e)–(h). physically, the filter center is on the blue side of the laser, that is, it has a higher frequency than the laser. However, feedback causes a red-shift of the instantaneous laser frequency. Eventually, when Δ is too large the laser is unable to support EFMs located around the center frequency of the filter, which means mathematically that the island actually shrinks down to a point and disappears. On the other hand, the stability region round the solitary laser frequency extends with increasing Δ to higher feedback rates κ, because the system now operates at the tail of the filter where the effective feedback rate is smaller. As a consequence, instabilities, such as the Hopf bifurcations bounding the stability region to the right, arise only for quite high levels of feedback κ.

We find a similar global transition in Fig. 3.6 where we decrease the detuning Δ from zero. In the individual panels of Fig. 3.6 the detuning has the same modulus as in the respective panels of Fig. 3.5 (only the sign has changed). This allows one to study the difference between positive and negative detuning. The effect of decreasing the detuning is qualitatively the same. In particular, the EFM region splits into two separate regions where the 'island' located around the center frequency of the filter is now at the top of the figure. Furthermore, the region of stable EFMs centered around the solitary laser frequency extends to higher values of κ with decreasing Δ. However, there are quite significant quantitative differences between Figs. 3.5 and 3.6. In particular, the separate island of stable EFMs around the center frequency of the filter is notably larger for negative detunings. This is due to the filter being on the red side of the laser. In combination with the red-shift of the solitary laser frequency caused by the feedback this leads to a large region of stability of these EFMs.

3.3. Transitions through codimension-three bifurcations. The boundary of the stable EFM regions is formed by either saddle-node bifurcation curves or by Hopf bifurcation curves. The switch-over points from one type of boundary to the other are codimension-two bifurcation points, namely either a Bodganov-Takens (BT) bifurcation or a saddle-node Hopf (SH) point. As was already mentioned in the previous section, we find that the BT point appears as 'switch-over' point only for sufficiently large Δ. The transition from an SH point to a BT switch-over point involves codimension-three bifurcations as is shown in Fig. 3.7. Panel (a) shows a situation as in Fig. 3.5(a), where the switch-over from saddle-node to Hopf bifurcation is due to a saddle-node Hopf point. Notice a second Hopf bifurcation curve that passes close to the saddle-node curve. The inset shows the frequency of the periodic orbit along this curve. As Δ is increased, the second Hopf curve becomes tangent

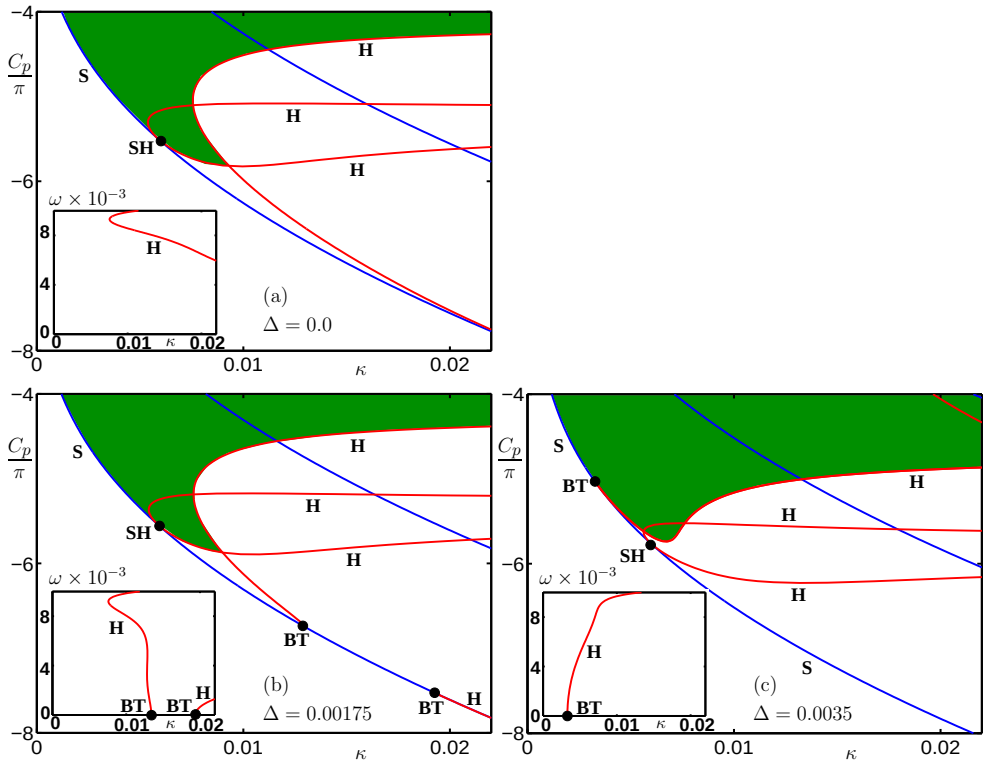

FIG. 3.7. *Enlarged views of bifurcation diagrams in the (κ, C_p)-plane near the creation of two Bogdanov-Takens (BT) points. The insets of each panel shows the frequency of the periodic orbits along branches of Hopf bifurcations, which goes to zero at the Bogdanov-Takens points.*

to the saddle-node curve at a degenerate Bogdanov-Takens point [3], after which it splits up and ends at two newly created BT points. That these points are indeed Bogdanov-Takens points is evidenced by the inset, which shows that the frequency of the respective periodic orbits goes to zero at the BT points as is demanded by theory. As Δ is increased further, one BT point moves to the right and out of the region of consideration, while the other BT point moves to the left. It eventually passes through the point SH at another codimension-three bifurcation, namely a Bogdanov-Takens-Hopf bifurcation where there is a semi-simple double eigenvalue and a pair of complex eigenvalues with zero real part. To our knowledge this bifurcation with a center manifold of dimension four has not been unfolded in the literature. In the present situation the BT point 'moves through' the SH point, so that it forms the switch-over point from now on; see Fig. 3.5(c).

The second transition involving codimension-three bifurcations that we discuss here in detail concerns the mechanism in which the single region of EFM stability splits up into two separate regions. Enlarged views near this splitting are shown in Fig. 3.8. In panel (a) there is still a narrow channel connecting the two parts of the EFM stability region. As Δ is increased, a saddle-node curve and a Hopf curve become tangent at a degenerate saddle-node Hopf point DSH [22]; see panel (b). When Δ is increased further, two codimension-two saddle-node Hopf points are created, each of which is now a switch-over point; see panel (c). This creates two separate EFM

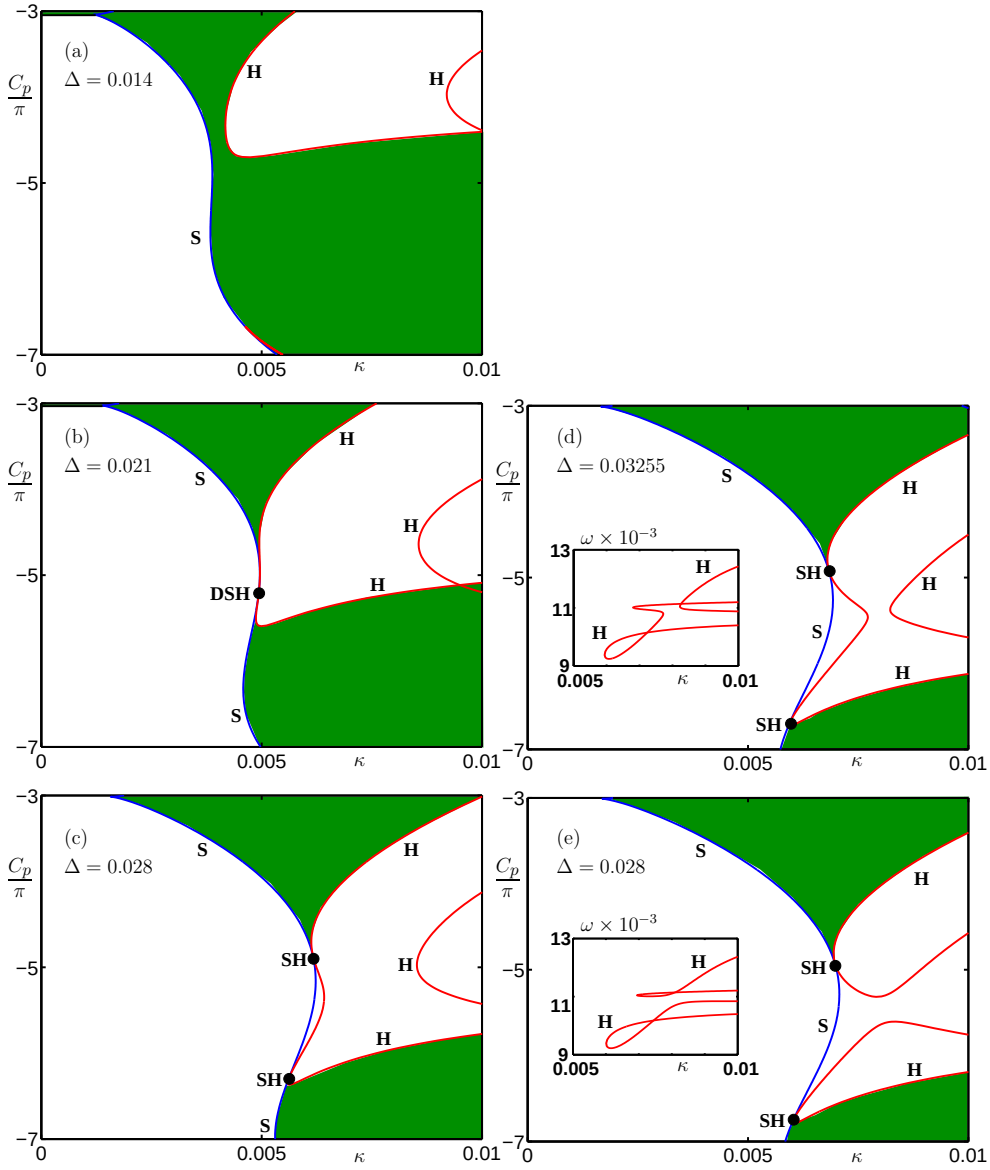

FIG. 3.8. *Enlarged views of bifurcation diagrams in the (κ, C_p)-projection near the splitting-off of the EFM stability region. The insets of panels (d) and (e) show the frequencies of the periodic orbits along the Hopf curves involved in a singularity transition.*

stability regions, one around the solitary laser frequency and one around the center frequency of the filter. Physically this corresponds to a level of detuning that is so large that the system cannot support 'mixed' EFMs with frequencies in between the solitary laser frequency and the center frequency of the filter any longer.

When Δ is increased further we find a transition through a saddle in the surface of Hopf bifurcations in (κ, C_p, Δ)-space. This manifests itself here as a change in how four branches of Hopf bifurcations connect; see the transition shown in Fig. 3.8(d) and (e). SPecifically, two Hopf curves approach each other, connect in a different

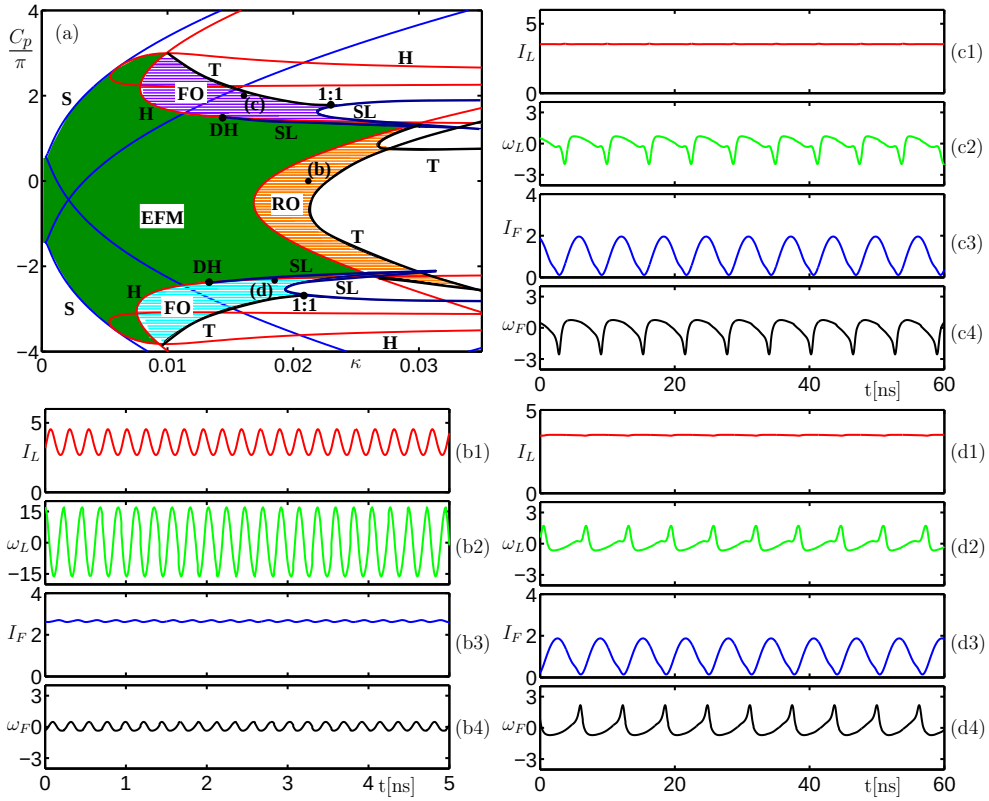

FIG. 4.1. *Panel (a) shows the two-parameter bifurcation diagram in the* (κ, C_p)*-plane for* $\Delta = 0$ *with different stability regions, namely, of EFMs (green), of ROs (orange), and of FOs (cyan and purple); boundaries are formed by saddle-node (S), Hopf (H), saddle-node of limit cycles (SL), and torus (T) bifurcations; shown are also 1:1-resonance and degenerate Hopf (DH) points. The black dots labeled (b), (c) and (d) are the parameter values of the time series in panels (b)–(d), which show the laser intensity* I_l*, the laser frequency* ω_L *(in units of* 10^9*), the filter intensity* I_F*, and the filter frequency* ω_F *(in units of* 10^9*). Case (b) shows ROs, and (c) and (d) show two examples of FOs.*

way and then separate again. As a result, the two SH points now lie on two different (unconnected) Hopf bifurcation curves. This 'completes' the splitting of the EFM stability islands that was discussed in the previous section.

4. Different types of oscillations. In laser systems with delayed feedback one can identity different characteristic time scales. From the physical point of view, one expects these time scales to show up as frequency components in the dynamics. In the FOF laser at least two time scales can be identified, one related to the solitary laser and a second related to the delay time.

A typical type of oscillation that one expects in any laser system are the so-called relaxation oscillations or ROs — a periodic exchange of energy between the optical field and the population inversion. In a solitary laser they are damped, but can be excited by a perturbation after which the laser relaxes down to constant output, hence, the name relaxation oscillation. They are fast oscillations. In the solitary laser their frequency is given by $\omega_{RO} = \sqrt{\frac{2P}{T}}$, where P is the pump rate and T the photon life time.

Since we are dealing with a laser with optical feedback, one also expects to find oscillations with a frequency of $\omega_{FO} \approx 2\pi/\tau$ where τ is the delay time. In other words, the time it takes for one external roundtrip of the light. These type of external roundtrip oscillations have been found experimentally in the FOF laser. Surprisingly, they have the feature that oscillations occur only in the laser frequency while the laser intensity remains practically constant [9]. This type of frequency oscillations or FOs are 'untypical' for semiconductor lasers, which are characterized by a strong coupling between amplitude and phase of the electric field (as expressed by large values of the parameter α, typically well above 1). In other words, one would expect any frequency oscillation to be accompanied by intensity oscialltions of a similar amplitude.

In this section we perform a detailed bifurcation analysis of the periodic orbits that are born when the EFMs become unstable in Hopf bifurcations. We determine which type of oscillations, ROs and FOs, appear where and determine their stability. In particular, we show that FOs are stable in large, experimentally accessible regions of the (κ, C_p)-plane. In fact, they are the dominamt type of oscillations for moderate levels of detunining Δ.

Figure 4.1(a) shows the bifurcation diagram in the (κ, C_p)-plane for $\Delta = 0$. As expected, the Hopf bifurcations bounding the EFM stability region give rise to oscillations, which are stable in the colored regions. There is a region (orange) of stable ROs, which can be accessed simply by following the solitary laser solution (around $C_p = 0$) towards higher levels of feedback strength κ. The region of stable ROs is bounded to the right by torus bifurcation curves. Furthermore, there are two regions (cyan and purple) of stable FOs in Fig. 4.1(a). We note that the two regions of FOs are almost mirror images of each other under reflection around the central frequency of the filter. This indicates that the amplitude-phase coupling (the parameter α) has only a small influence; see also [27]. However, note that the stability region of ROs is actually quite asymmetrical in Fig. 4.1(a). Another important feature is that stable FOs occur for much lower levels of κ than ROs.

The FO stability regions are bounded to the right by torus and saddle-node of limit cycle bifurcations. The torus curves emerge from double Hopf points and meet the SL curves at 1:1 resonance points. These regions have been determined by computing many one-parameter cross sections for fixed C_p and continuing with DDE-BIFTOOL the respective solutions in κ; see also Section 5. In fact, the horizontal colored lines in Fig. 4.1 are actual branches of stable periodic orbits. The codimension-one bifurcation curves of periodic orbits, T and SL, were found as bifurcation points on the one-parameter branches and continued directly with PDDE-CONT [30].

Figure 4.1 also shows examples of oscillations in the three different stability regions. In each case we show time series of the laser intensity I_l, the laser frequency ω_L, the filter intensity I_F, and the filter frequency ω_F. Panels (b) shows a typical example of ROs where both the laser intensity I_l and the laser frequency ω_L oscillate. For the (typical) laser parameters considered here the ROs have a physical RO frequency of 4.21 GHz. Note that ROs hardly show any dynamics of the filter — it remains more or less passive.

Figure 4.1 (c) and (d) are examples of FOs, which are clearly external roundtrip oscillations with a frequency on the order of $1/\tau$, that is, they are much slower than ROs (note the different scale on the time axis). Furthermore, the laser intensity is almost constant for FOs (certainly compared to ROs). However, we find dynamics in the filter field — both in the filter intensity I_F and the filter frequency ω_F. In other words, the filter effectively compensates for the intensity dynamics that one would

normally expect in a semiconductor laser. The difference between the FOs shown in Fig. 4.1(c) and (d) is the phase relationship between the laser frequency ω_L and the feedback intensity I_F. For the FOs shown in panel (c), from the upper (purple) FO stability region of panel (a), ω_L and I_F are almost in phase. This is in accordance with the fact that they oscillate around the left flank of the filter, where an increase of the frequency ω_L results in increased transmission of the intensity I_F. For the FO shown in panel (d), from the lower (cyan) FO region of panel (a), on the other hand, ω_L and I_F are almost in anti-phase. This time the oscillations are around the right flank of the filter, so that I_F decreases as ω_L increases.

4.1. Dependence of RO and FO stability on the detuning. The strong influence of the detuning Δ on the EFM stability regions that was discussed in Section 3.2 is mirrored by a strong influence on the stability regions of ROs and FOs.

Figure 4.2 shows the bifurcation diagram in the (κ, C_p)-plane for three positive values of Δ. As the detuning is increased, the RO stability region (orange) becomes smaller and moves towards lower values of C_p, but overall does not change very much. Notice that ROs appear only when EFMs located around the central frequency of the filter become unstable. The influence on the FO stability regions of changing Δ is much more dramatic. The lower (cyan) FO stability region decreases significantly in size and then disappears entirely; see Fig. 4.2(b) and (c). On the other hand, the upper (purple) FO stability region grows substantially in size; see panel (b). For larger values of Δ this FO stability region occupies a substantial area between the two separate EFM stability regions; see panel (c). It is bounded in the 'EFM stability gap' by a curve SL of saddle-node bifurcations of limit cycles on the left. Its right boundary also becomes much more complicated. For sufficiently large Δ we find that FOs may become unstable in period-doubling bifurcations, so that we find regions of stable period-doubled FOs.

Throughout the whole region the approximate in-phase relationship between ω_L and I_F is preserved. This is because the stable FO region never extends to the other side of the filter flank. However, in Fig. 4.2(b), new oscillations become stable and coexist with the upper stable FO region. There is a small region around $(\kappa, C_p) = (0.01, 1)$ where faster FOs are stable, they feature a period $T_{FO} \approx \tau/2$. This region becomes larger for even larger detuning; see Fig. 4.2(c). Initially, for $\Delta = 0.014$ in Fig. 4.2(b), these fast FOs are created in super-critical Hopf bifurcations of EFMs. They destabilize in torus bifurcations T as C_p is decreased and in sub-critical period-doubling bifurcations (P) as κ is increased. For larger detuning, $\Delta = 0.0315$ in Fig. 4.2(c), there are already two regions of fast FOs. The upper one features a period of $T_{FO} \approx \tau/4$ and undergoes a torus bifurcation for increasing κ. The lower one features a period of $T_{FO} \approx \tau/2$, undergoes a sub-critical period doubling bifurcation and connects to the large FO region. This will be discussed in more detail in Section 5.

Figure 4.3 shows the bifurcation diagram in the (κ, C_p)-plane for three different values of negative detuning. (Compare also with Fig. 5.1(a) and Fig. 4.2(a) and (b).) Again we find a large region of stable ROs around the filter center. Similar to Fig. 5.1(a), there are still two regions of stable FOs; in the upper (purple) region there is an in-phase relationship between ω_L and I_F (left flank of the filter profile), while in the lower (cyan) region there is an anti-phase relationship between ω_L and I_F (right flank of the filter). However, when Δ is decreased, the (purple) region of stable in-phase FOs increases in size, whereas the (cyan) region of stable anti-phase FOs becomes smaller and then disappears; see Fig. 4.3(b) and (c). As a result, the regions of stable anti-phase FOs extend over a large area in the (κ, C_p)-plane, between the

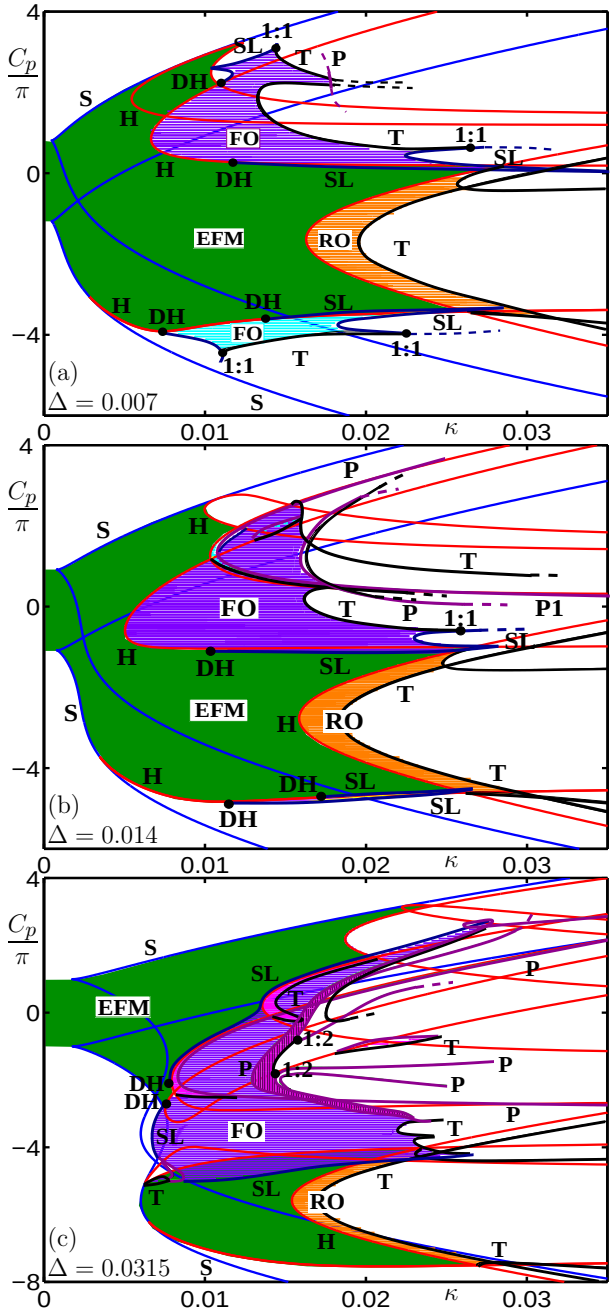

FIG. 4.2. *Two-parameter bifurcation diagram in the (κ, C_p)-plane for increasing detuning Δ as indicated in the panels; notation is as in Fig. 4.1 with the addition of period doubling (P) bifurcations.*

regions of stable EFMs. As is the case for positive Δ, this large FO stability region is characterized by the appearance of period-doubled solutions. In terms of the EFM and FO stability regions, the panels of Fig. 4.3 for negative Δ are almost reflected images of those in Fig. 4.2 positive Δ. This again highlights the weak influence of the amplitude-phase coupling parameter α on these dynamics.

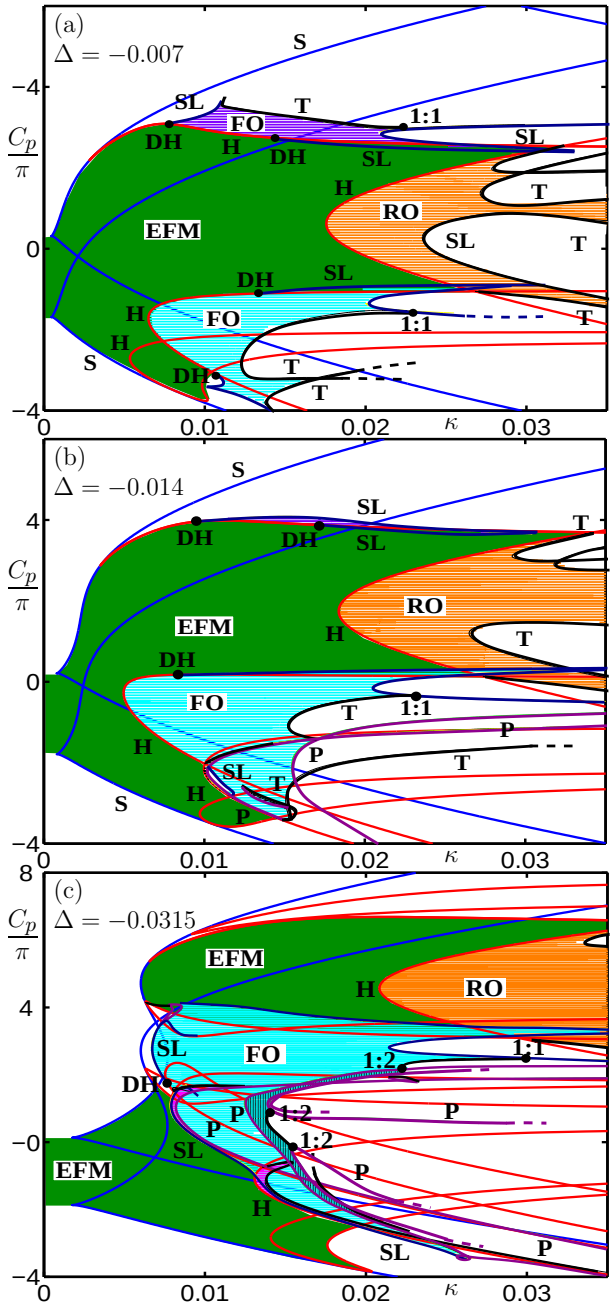

FIG. 4.3. *Two-parameter bifurcation diagram in the (κ, C_p)-plane for decreasing detuning Δ as indicated in the panels; notation is as in Fig. 4.1 with the addition of period doubling (PD) bifurcations.*

5. Beyond stable frequency oscillations. Evidence of possible period-doublings of FOs has been found experimentally [6], and our bifurcation analysis shows that regions of stable period-doubled FOs do exist for sufficiently large detuning Δ. We now consider this transition of FOs in more detail. Figure 5.1(a1) shows a one-parameter bifurcation diagram, where we plot branches of EFMs and FOs as a function of κ

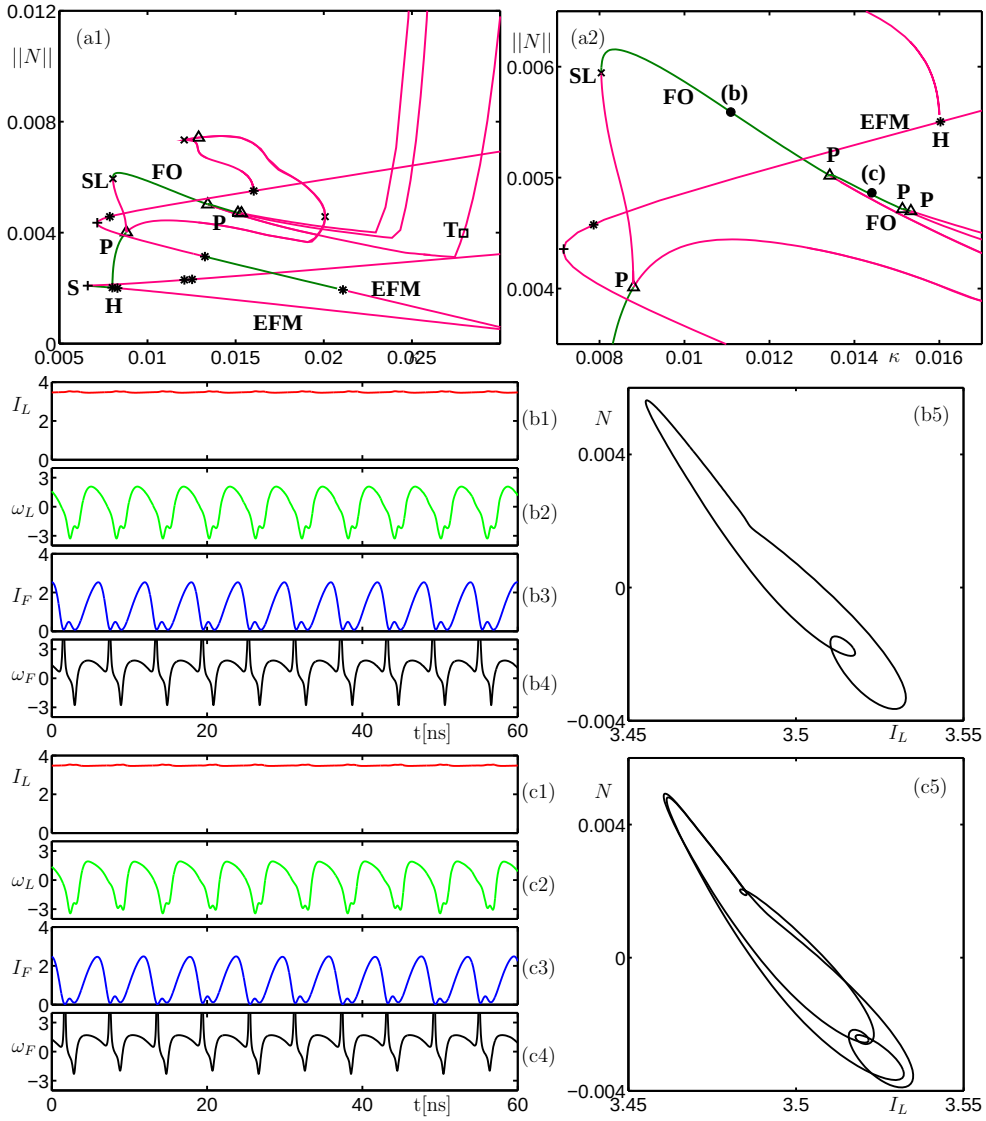

FIG. 5.1. *Panel (a1) shows a one-parameter bifurcation diagram in the parameter κ for fixed $(\Delta, C_p) = (0.0315, -2.26\pi)$. As is clear from the enlargement in panel (a2), there is a region of stable period-doubled FOs after the first period-doubling bifurcations (P) of a period-doubling cascade. Labels (b) and (c) indicate points on the FO branch for which time series and phase portraits are shown in panels (b) and (c).*

for fixed $(\Delta, C_p) = (0.0315, -2.26\pi)$. Figure 5.1(a2) is an enlarged view around a period-doubling cascade of FOs. The appearance of stable period-doubled FOs is actually not so straightforward. A stable EFM undergoes a Hopf bifurcation H, from which a branch of FOs emerges with a period of around $\tau/2$. This branch of periodic orbits then undergoes a subcritical period-doubling bifurcation P. (Note that, after further bifurcations, this branch connects to a second Hopf bifurcation on a different EFM branch.) The initially unstable period-doubled periodic orbit stabilizes in a

saddle-node of limit cycle bifurcation SL. The period of these stable FOs is now approximately τ, and this part of the branch lies in the (purple) FO stability region in Fig. 4.2(c). This branch destabilizes in another period-doubling bifurcation P, which is the first in a cascade of supercritical period-doublings.

Figure 5.1(b1)–(b4) shows time series and Fig. 5.1(b5) the corresponding trajectory in the (I_L, N)-plane for the point on the main stable FO branch; labeled (b) in panel (a2). As is typical for FOs, the laser intensity I_L is almost constant. Note the small scale of the x-axis in Fig. 5.1(b5). The inversion N of the laser is directly related to the laser frequency ω_L. Figure 5.1(c1)–(c4) are time series and Fig. 5.1(c5) is a trajectory in the (I_L, N)-plane for a point on the stable period-doubled FO branch; labeled (c) in panel (a2). The time series look quite similar to the ones in Fig. 5.1(b) and, in particular, the intensity I_L is still virtually constant. However, as is most prominent in the frequency dynamics of the laser, it can be seen that any two consecutive dips of ω_L are no longer identical. Indeed the period of oscillations is now about twice what it was before in panels (b). Also the phase portrait in Fig. 5.1(c5) shows that the periodic orbit has period-doubled.

We now discuss another way in which FOs can become unstable. This is related to the question of whether it is possible to have a 'mixing' of features of FOs and of ROs. One would expect to find such mixed types of oscillation near the double-Hopf points, that is, where the boundaries of the stability regions of FOs and ROs come together. Figure 5.2 shows an example of a stable FO (an external roundtrip oscillation of period about τ) that shows small oscillations with the typical and much faster RO frequency. Panel (a) is a one-parameter bifurcation diagram, where we plot branches of EFMs and FOs as a function of κ for fixed $(\Delta, C_p) = (0.0315, -4\pi)$. The inset shows the period of the periodic orbit along the FO branch. Starting from a Hopf bifurcation H, of an unstable EFM around $(\kappa, ||N||) \approx (0.009, 0.0041)$, a branch of unstable FO emerges. After undergoing several saddle-node of limit cycle bifurcations SL it eventually becomes stable. The stable part of the FO branch is almost horizontal until, for a higher feedback rate around $\kappa = 0.0225$, the norm $||N||$ increases dramatically. This is a smooth transition and not a bifurcation, even though it looks very sudden in this projection. (Note that the FO period does not show such a sudden change.)

To explain the increase of the norm $||N||$ we note a Hopf bifurcation on the lower part of the EFM branch in Fig. 5.2(a), which gives rise to unstable ROs. The corresponding EFM of saddle type is, therefore, characterized by leading complex conjugate unstable eigenvalues whose imaginary parts are close to the RO frequency (which is very typical in semiconductor laser systems). The idea is that, when it comes near this EFM, that the FO 'picks up' the additional RO frequency that soon renders the FO branch unstable in a torus bifurcation T. Consequently, these oscillations of increasing amplitude make a substantial and increasing contribution to the norm $||N||$ along the FO branch, which leads to its increase.

To illustrate this further, Fig. 5.2(b) shows time series of the FOs for parameter values identified by the black dot close to the torus bifurcation T in panel (a). Note again that the power is still almost constant, but additional fast oscillations are clearly seen in the frequency ω_L of the laser. That these are indeed on the scale of the ROs is demonstrated by the gray time series in panels (b). These are for parameter values identified by the black dot on the RO curve in panel (a). Moreover, the FO time series are split up into blue, red and black parts to highlight different sections of the trajectory. During the blue interval a fast oscillation is building up, which decays

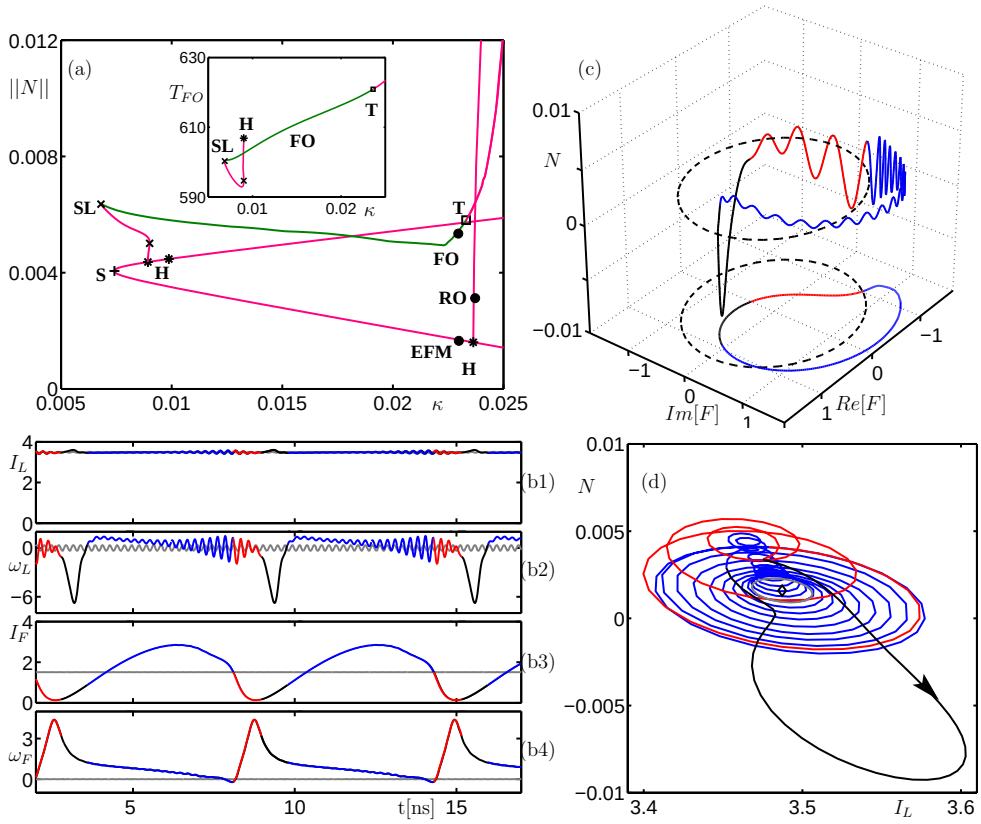

FIG. 5.2. *Panel (a) shows a one-parameter bifurcation diagram in the parameter κ for fixed $(\Delta, C_p) = (0.0315, -4\pi)$. The inset shows the period T_{FO} along the branch of FOs, which are stable between in saddle-node of limit cycle (SL) and a torus (T) bifurcation. Panels (b) shows time series of the stable periodic orbit for $\kappa = 0.0226$ (black dot in panel (a) near the end of the FO stability region). Along the blue part there is a build-up and along red part a decay of fast oscillations, and the black part is a global excursion; for comparison an unstable relaxation oscillation (that appears for slightly higher κ) is shown as the gray time series in panels (b). Panel (c) shows the trajectory in the (F, N)-space and its projection on the F-plane; the dashed line in panel (c) indicates the unstable EFM. Panel (d) shows the projection on the (I_L, N)-plane. The diamond is the unstable EFM and the gray circle is the trajectory of the unstable ROs.*

again during the red interval. The build-up rate is noticeably slower than the decay rate. During the black interval the trajectory makes a large excursion in phase space.

The FO periodic orbit is shown in Fig. 5.2(c) in the (F, N)-space and in the projection onto the F-plane, and in Fig. 5.2(d) in the projection onto the (I_L, N)-plane. The dotted circle in panel (c) indicates the position of the unstable EFM. (We remark that we fixed the phase of the periodic orbit, but still show the entire S^1 group orbit of the EFM for convenience.) Panel (c) shows that the change from build-up to decay of fast oscillations occurs when the trajectory is closest to the dotted circle representing the saddle EFM. This can be seen even better in the (I_L, N)-projection of Fig. 5.2(d). Now the EFM is indicated by a diamond and the orbit of the close-by unstable RO is shown in gray. The arrow indicates the direction along the periodic orbit.

A possible interpretation of the overall FO dynamics is the following. During the

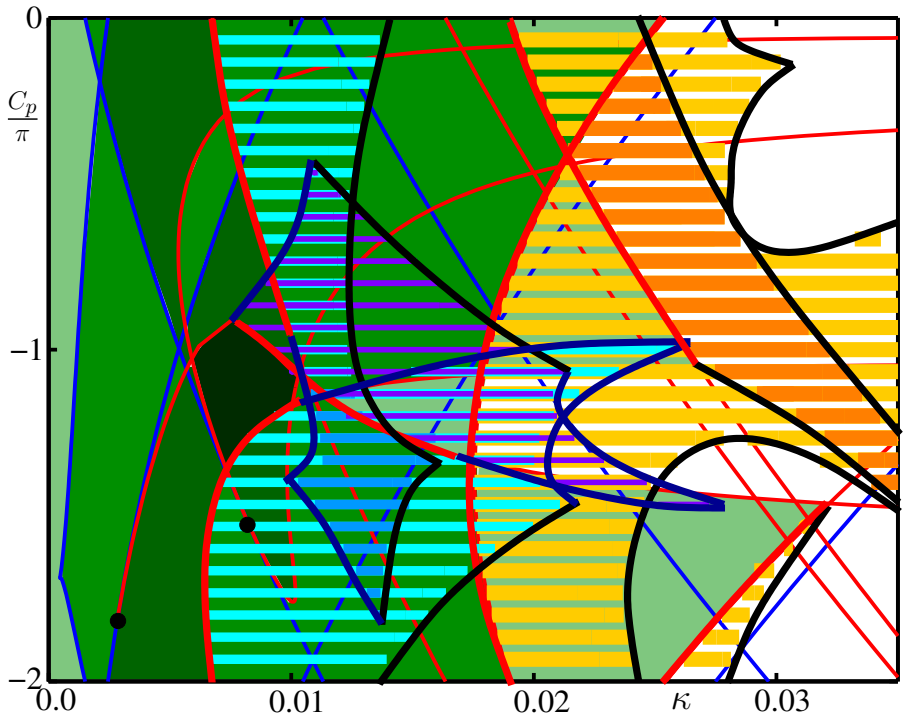

FIG. 6.1. *Two-parameter bifurcation diagram in the* (κ, C_p)*-plane for* $\Delta = -0.007$*, where all stability regions of EFMs, ROs and FOs are shown on a fundamental* 2π*-interval of* C_p*; compare with Figs. 3.3(a) and 4.1(a). The image summarizes the large amount of multistability of the FOF laser; the multistability of EFMs is indicated by different shades of green, that of of RO by different shades of orange, and that of FO by different shades of blue.*

blue build-up of oscillations the trajectory also comes closer to the saddle EFM. After its closest approach to the EFM the trajectory leaves again, but with a faster rate. This indicates that this motion is along certain directions on the stable and unstable manifolds of the EFM that are characterised by complex conjugate eigenvalues. The frequency of the oscillations remains practically constant and of the order of the ROs, which is arguably because the EFM is close to a Hopf bifurcation of an also unstable RO. The black part of the trajectory is a large excursion in phase space that leads to a reinjection into the vicinity of the EFM. It seems that the FO periodic orbit is close to a heteroclinic connection with the EFM, but such details of the dynamics are beyond the scope of this paper. Nevertheless, Fig. 5.2 is a clear example that mixed FO/RO dynamics can be found in the FOF laser system.

6. Summary and outlook. We have investigated the bifurcation structure of a semiconductor laser with filtered optical feedback (FOF) as a function of three main parameters, namely the feedback rate κ, the feedback phase C_p, and the detuning Δ between the solitary laser frequency and the center frequency of the filter. The emphasis here was on stable external filtered modes and bifurcating stable oscillations, which can either be relaxation oscillations or frequency oscillation. This stability information was presented by two-parameter bifurcation diagrams in the (κ, C_p)-plane for different, representative values of Δ. Depending on the value of Δ, we found a

single or two separate large regions of stable EFMs. Our results show clearly that the feedback phase C_p is a key parameter in the FOF laser. In other words, both the *magnitude* and the *phase* of the complex feedback parameter κe^{iC_p} must be considered to reveal a comprehensive picture of the dynamics.

It is convenient to represent the results in the covering space of C_p, that is, over several 2π-periods of C_p. In this way, one can follow a particular solution, for example, the solitary laser solution for $\kappa = 0$, to the different stability boundaries. This agrees with the physical point of view because it corresponds to what one does in an experiment: one follows a known solution in parameters. Note that the feedback strength κ and the feedback phase C_p can be changed independently and 'on-line' in an experiment. In fact, the bifurcation diagrams in Figs. 4.2 and 4.3 form the basis for ongoing measurements of the FOF laser with the goal of characterizing experimentally the stability boundaries of the regions of stable ROs and FOs.

Our theoretical study produced specific results concerning these two types of oscillations, which will inform the experiments. Stable ROs are generally found near the center frequency of the filter. Physically, the effective instantaneous feedback is highest around the center frequency of the filter, irrespective of the detuning Δ. In fact, the size and the shape of the stable RO region does change with Δ. Frequency oscillations, on the other hand, are substantially different — the interaction between the laser and the filter is vital for their existence. We find (for Δ close to zero) two separate regions of stable FOs, namely, in-phase and anti-phase dynamics between laser and filter, which occur at the two opposite flanks of the filter profile. All FOs have in common that the laser intensity is almost constant. For larger detunings Δ we find a single large region of stable FOs in between the two separate EFM stability regions. Importantly, FOs can be found already for quite low values of κ.

The presentation of bifurcation diagrams in the covering space is very convenient for orientation purposes, especially in an experiment. However, it does not convey the strong multistability of the FOF laser. We finish by giving an idea of the overall complexity of the FOF laser system in Fig. 6.1, where all stability regions of EFMs, ROs and FOs are shown on a fundamental 2π-interval of C_p. Effectively, every dynamical state can coexist with any other one in some region of the (κ, C_p)-plane. Figure 6.1 also demonstrates the advantage of bifurcation analysis of DDEs with numerical continuation tools over numerical simulation. By tracking individual solutions in the relevant parameters we were able to detect multistability reliably. By contrast, it would be very difficult to ensure that all simultanous attractors are found with numerical simulation.

Laser systems with delay have been a class of motivating testbed examples for the recent development of computational tools for DDEs [20]. The bifurcation study presented here is much in this spirit in that it demonstrates the state-of-the-art of numerical continuation techniques for DDEs arising in applications. We hope that numerical methods of bifurcation analysis will find use in other areas of application where delays are important, such as control theory, ecological systems and network dynamics, to name just a few.

Acknowledgements. We thank Kirk Green for helpful discussions and comments on a manuscript of this work.

REFERENCES

[1] D. H. DeTienne, G. R. Gray, G. P. Agrawal, and D. Lenstra, *Semiconductor laser dynamics for feedback from a finite-penetration-depth phase-conjugate mirror*, IEEE J. Quantum Electron., 33 (1997), pp. 838–844.

[2] O. Diekmann, S. A. V. Gils, and S. M. V. Lunel, *Delay Equations: Functional-, Complex-, and Nonlinear Analysis*, Springer Verlag, New York, 1995.

[3] F. Dumortier, R. Roussarie, J. Sotomayor, and H. Zoladek, *Bifurcations of Planar Vector Fields. Nilpotent Singularities and Abelian Integrals*, vol. 1480 of Lecture Notes in Math., Springer-Verlag, Berlin, 1991.

[4] K. Engelborghs, T. Luzyanina, and G. Samaey, *DDE-BIFTOOL v. 2.00 user manual: a matlab package for bifurcation analysis of delay differential equations.*, Technical Report TW-330, Department of Computer Science, K. U. Leuven, Leuven, oct 2001.

[5] T. Erneux, M. Yousefi, and D. Lenstra, *The injection laser limit of lasers subject to filtered optical feedback*, in Proc. European Quantum Electronics Conf., 2003.

[6] H. Erzgräber, B. Krauskopf, D. Lenstra, A. P. A. Fischer, and G. Vemuri, *Frequency versus relaxation oscillations in a semiconductor laser with coherent filtered optical feedback*, Applied Nonlinear Mathematics Research Report, University of Bristol, 2005.24 (2006).

[7] B. Farias, T. P. de Silans, M. Chevrollier, and M. Oriá, *Frequency bistability of a semiconductor laser under a frequency-dependent feedback*, Phys. Rev. Lett., 94 (2005), p. 173902.

[8] A. P. A. Fischer, O. K. Andersen, M. Yousefi, S. Stolte, and D. Lenstra, *Experimental and theoretical study of filtered optical feedback in a semiconductor laser*, IEEE J. Quantum Electron., 36 (2000), pp. 375–384.

[9] A. P. A. Fischer, M. Yousefi, D. Lenstra, M. W. Carter, and G. Vemuri, *Experimental and theoretical study of semiconductor laser dynamics due to filtered optical feedback*, Phys. Rev. Lett., 92 (2004), pp. 023901–023904.

[10] K. Green and B. Krauskopf, *Bifurcation analysis of a semiconductor laser subject to non-instantaneous phase-conjugate feedback*, Opt. Commun., 231 (2004), pp. 383–393.

[11] K. Green and B. Krauskopf, *Mode structure of a semiconductor laser subject to filtered optical feedback*, Opt. Commun., 258(2) (2006), pp. 243–255.

[12] K. Green and B. Krauskopf, *Analysis of the external filtered modes of a semiconductor laser with filtered optical feedback*, in: Semiconductor Lasers and Laser Dynamics II, Proceedings of SPIE (D. Lenstra, M. Pessa and Ian H. White; Eds.), 6184-30 (to appear).

[13] J. Guckenheimer and P. Holmes, *Nonlinear Oscillations, Dynamical Systems, and Bifurcations of Vector Fields*, Springer-Verlag, New York, 1986.

[14] B. Haegeman, K. Engelborghs, D. Rose, D. Pieroux, and T. Erneux, *Stability and rupture of bifurcation bridges in semiconductor lasers subject to optical feedback*, Phys. Rev. E, 66 (2002), p. 046216.

[15] J. K. Hale and S. M. V. Lunel, *Introduction to Functional Differential Equations*, Springer Verlag, New York, 1993.

[16] E. Hecht, *Optics*, Addison Wesley, London, UK, 2002.

[17] G. Hek and V. Rottschäfer, *Semiconductor laser with filtered optical feedback: bridge between conventional feedback and optical injection*, in Proc. ENOC, vol. to appear, 2005.

[18] G. Hek and V. Rottschäfer, *Frequency versus relaxation oscillations in a semiconductor laser with coherent filtered optical feedback*, submitted, (2006).

[19] D. M. Kane and K. A. Shore (Eds.), *Unlocking Dynamical Diversity: Optical Feedback Effects on Semiconductor Lasers*, Wiley, 2005.

[20] B. Krauskopf, *Bifurcation analysis of lasers with delay*, in Unlocking Dynamical Diversity: Optical Feedback Effects on Semiconductor Lasers, D. Kane and K. Shore (Eds.), New York, 2005, Wiley, pp. 147–183.

[21] B. Krauskopf and D. Lenstra (Eds.), *Fundamental Issues of Nonlinear Laser Dynamics*, AIP Conference Proceedings Vol. 548, Melville, New York, 2000.

[22] B. Krauskopf and C. Rousseau, *Codimension-three unfoldings of reflectionally symmetric planar vector fields*, Nonlinearity, 10(5) (1997), pp. 1115–1150.

[23] B. Krauskopf, G. V. Tartwijk, and G. Gray, *Symmetry properties of lasers subject to optical feedback*, Opt. Commun., 177 (2000), pp. 347–353.

[24] Yu. A. Kuznetsov, *Elements of Applied Bifurcation Theory*, Springer-Verlag, New York, 1995.

[25] L. Larger, P.-A. Lacourt, S. Poinsot, and M. Hanna, *From flow to map in an experimental high-dimensional electro-optic nonlinear delay oscillator*, Phys. Rev. Lett., 95 (2005), p. 043903.

[26] D. Lenstra and M. Yousefi, *Theory of delayed optical feedback in lasers*, in Fundamental Issues of Nonlinear Laser Dynamics, B. Krauskopf and D. Lenstra, eds., vol. 548 of AIP Conference Proceedings, New York, 2000, pp. 66–86.

[27] M. Nizette and T. Erneux, *Semiconductor lasers subject to weak filtered optical feedback: an analytical study*, submitted, (2006).

[28] F. Rogister, P. Mégret, O. Deparis, M. Blondel, and T. Erneux, *Suppression of low frequency fluctuations and stabilization of a semiconductor subject to optical feedback from a double cavity: Theoretical results*, Opt. Lett., 24 (1999), pp. 1218–1220.

[29] V. Rottschäfer and B. Krauskopf, *The ecm-backbone of the lang-kobayashi equations: a geometric picture*, Applied Nonlinear Mathematics Research Report, University of Bristol, 2005.20 (2005).

[30] R. Szalai, *PDDE-CONT: A continuation and bifurcation software for delay-differential equations*, Department of Applied Mechanics, Budapest University of Technology and Economics, `http://www.mm.bme.hu/ szalai/pdde`, Budapest, Hungary, 2005.

[31] V. Z. Tronciu, H.-J. Wünsche, M. Radziunas, and M. Wolfrum, *Semiconductor lasers under resonant feedback from a fabry–perot: Stability of continuous wave operation*, WIAS Preprint, 1051 (2005).

[32] S. M. Wieczorek, B. Krauskopf, T. B. Simpson, and D. Lenstra, *The dynamical complexity of optically injected semiconductor lasers*, Physics Reports, 416(1-2) (2005), pp. 1–128.

[33] A. Yariv, *Quantum Electronics*, John Wiley and Sons, New York, 1988.

[34] M. Yousefi, D. Lenstra, and G. Vemuri, *Nonlinear dynamics of a semiconductor laser with filtered optical feedback and the influence of noise*, Phys. Rev. E, 67 (2003), p. 046213.

[35] M. Yousefi, D. Lenstra, G. Vemuri, and A. P. A. Fischer, *Control of nonlinear dynamics of a semiconductor laser with filtered optical feedback*, in IEE Proc. Optoelectron., vol. 148, 2001, pp. 223–237.